Improving the technique for controlled cryogenic destruction of conjunctival tumors located in the projection of the ciliary body onto the sclera: a preliminary report

O.S. Zadorozhnyy[1], Cand Sc (Med); **N.V. Savin**[2], Cand Sc (Techn); **A.S. Buiko**[1], Dr Sc (Med), Prof

[1] Filatov Institute of Eye Diseases and Tissue Therapy, NAMS of Ukraine;
Odessa (Ukraine)

[2] Municipal Clinical Hospital No.1;
Odessa (Ukraine)

E-mail: laserfilatova@gmail.com

Background: *In case of controlled cryogenic destruction of an epibulbar tumor, making direct temperature measurements in the tumor and surrounding tissues during the treatment process is difficult and dangerous. Infrared thermography (IRT) is, however, capable of imaging and recording only superficial-tissue temperature changes. Mathematical modeling can be used to assess the temperature distribution in the underlying structures based on their thermal physical characteristics.*
Purpose: *To develop a model for temperature distribution in the ocular tunics in cryogenic destruction of conjunctival tumors located within a zone involving the ciliary body, in order to determine the tunic freezing parameters enabling reduced risk of complications while meeting the principles of ablastics.*
Materials and Methods: *Twenty-five patients (25 eyes) underwent real-time IRT during controlled cryogenic destruction of benign and malignant epibulbar lesions located in the projection of the ciliary body onto the sclera. A model for temperature distribution in the ocular tunics in cryogenic destruction of conjunctival tumors located within a ciliary body zone was implemented using Microsoft Quick BASIC Version 4.5.*
Results: *IRT-based analysis of temperature distribution found that, in cryogenic destruction of epibulbar tumors located in the projection of the ciliary body onto the sclera, initially, the sclera surrounding the centre of exposure gradually cooled down, while the cornea started cooling down rapidly only in 30 to 60 seconds, depending on tumor size and cryogenic unit parameters. The model (a) was developed while taking into account differences in heat conduction and heat capacity between the sclera, ciliary body and cornea, and (b) was also in agreement with the above finding.*
Conclusion: *The method for IRT-based temperature field monitoring in cryogenic destruction of epibulbar tumors, and the thermal physical model developed will allow determining the individual cryogenic exposure parameters that would prevent excessive freezing of the surrounding structures (in particular, the ciliary body and corneal endothelium). IRT allows for the assessment of post-freezing increases in ocular tissue temperature to the baseline temperature, thus contributing to reduced complication rate, should a repeat cycle of cryogenic destruction of the tumor be required. Further studies should match individual cryogenic exposure durations computed by the model to the data relating to long-term clinical outcomes.*

Keywords:
epibulbar tumors, cryogenic destruction, infrared thermography, model

Introduction

Cryogenic destruction of conjunctival tumors is an effective treatment for the condition, associated with a low recurrence rate [1-3], and successfully used both as a stand-alone treatment (Fig.1) and in combination with other modalities [4-7].

Cryotherapy for the tumor located within a zone involving the ciliary body, limbus, and peripheral cornea (Fig. 2) in some cases may be followed by complications (keratitis, iritis, iridocyclitis, or uveitis with deformation of the pupil) owing to the duration of cryogenic exposure.

The importance of knowing the duration of cryogenic exposure for cryogenic destruction of tumors of any location has been acknowledged [8]. The duration depends on multiple factors, but mainly on the nature, size and location of the tumor. In order to determine the duration of cryogenic exposure while treating for eyelid skin tumors, we have used a model developed previously [9] which takes into account direct temperature measurements both of tumor tissues and adjacent healthy tissues during the process of cryogenic destruction.

However, in case of cryogenic destruction of an epibulbar tumor, making direct temperature measurements in the tumor tissue and especially surrounding tissues during the treatment process is difficult and dangerous, and a non-invasive approach is required. Such an approach was rather surprisingly found while recording scleral-surface infrared thermography (IRT) patterns during cryogenic destruction of epibulbar tumors located in the projection of the ciliary body onto the sclera. Interest of medical practitioners (including ophthalmologists) in applications of IRT has been renewed in recent years [10-12]. The modality is, however, capable of imaging and recording only superficial-tissue temperature changes during cryogenic destruction of the tumor. We found it reasonable to use mathematical modeling for the assessment of temperature distribution in the underlying structures (sclera, vitreous, and ciliary body) [13, 14]. Knowing temperature gradients of freeze zones for the epibulbar tumor located in the projection of the ciliary body onto the sclera will contribute to reduced rate of complications with improvement in treatment outcomes, while meeting the principles of ablastics.

The **purpose** of the study was to develop a model for temperature distribution in the ocular tunics in cryogenic destruction of conjunctival tumors located within a zone involving the ciliary body, in order to determine the tunic freezing parameters enabling reduced risk of complications while meeting the principles of ablastics.

Materials and Methods

Since October 2016, 25 patients (25 eyes) have undergone real-time IRT of the freeze zone during controlled cryogenic destruction of benign and malignant epibulbar lesions (melanoma, 10 cases; carcinoma, 8; dysplasia, 2; papilloma, 3; hemangioendothelioma, 1; and hemangiopericytoma, 1) located in the projection of the ciliary body onto the sclera.

A microcryogenic cylinder-and-throttle system capable of producing low temperatures within the range of -120…-90 °C depending on gas pressure in the cylinder was used to perform the destruction [15]. The cryogenic destruction methodology provided for stable freezing, with the duration of cryogenic exposure depending on the amount and location of tumor tissue, dimensions of cryogenic tip, and cryogen pressure. Double freeze-thaw cycles were performed in case of conjunctival melanoma.

A smartphone attached IRT system, FLIR ONE (FLIR® Systems, Inc., USA; spectral range, 8-14 μm) [16], was used for displaying the images of thermal patterns of the freeze zone. Although the temperature characteristics of FLIR ONE (temperature range, -20°C to +120°C) were, a priori, too low for enabling quantitative assessment of temperature distribution within the freeze zone, the pattern of temperature distribution was clearly seen.

Thermal parameters of the eye (scleral conjunctiva and cornea) were monitored before and after surgery. Images of thermal patterns were obtained. In addition, time of freezing and time of thawing with regard to external ocular surface structures (including the cornea) surrounding the center of freezing were recorded.

Examination and treatment of patients were performed under stable environmental conditions (air temperature and humidity control and minimal indoor air velocity). Patients spent 20 minutes indoors with their eyes closed for adaptation to the indoor environment prior to IRT.

This study followed the ethical standards stated in the Declaration of Helsinki and was approved by the Local Ethics Committee of the Filatov Institute. Written informed consent was obtained from all individual participants included in the study.

A model for temperature distribution in the ocular tunics in cryogenic destruction of conjunctival tumors located within a zone involving the ciliary body was implemented using Microsoft Quick BASIC Version 4.5 (Microsoft, Redmond, WA).

Clinical Stage Results

In a number of cases, the pattern of temperature distribution in the freeze zone was surprisingly found to change over time. Initially, the pattern took the shape of regular concentric circles spreading outward from the freeze center, but over time the circles started becoming irregular, with their circumferences extending towards the cornea. However, there were no substantial visual changes in the shape of the freeze zone.

Thus, initially, the sclera surrounding the centre of freezing was the first to gradually cool down, while the cornea started cooling down only in 30 to 60 seconds. In addition, the temperature of the central cornea decreased from 35.1±0.8 °C to 22.4±0.9 °C, whereas that of the corneal site adjacent to the tumor decreased to less than 10 °C. In each patient, individual gradual thawing-induced increases in tissue temperature in the exposure zone over time were recorded. The ocular surface temperature returned to baseline 10 minutes on average after the cryogenic destruction process was stopped and the eyelid retractor was removed.

Mathematical formulation

Choroidal circulation is known to be a key source of heat to the human eye. Blood entering the eye (a) has a temperature that is practically equal to that of the body, and (b) produces a temperature gradient between the choroid and cornea which induces a heat transfer from blood to ocular tissues [13, 17]. We hypothesize that the irregularities found in surface thermal patterns in the course of cryogenic destruction are caused by the fact that the ciliary body becomes occluded from the blood circulation, and the subsequent heat extraction becomes more active in structures of minimal circulation (the cornea). Therefore, the task to be accomplished is to determine a time point at which the initial freeze zone deformation that cannot be visually identified occurs in each specific case.

Knowing the anatomical structure of the human eye, thermophysical properties of ocular structures (Table 1), temperature characteristics of cryogenic tip, and the

size of the tumor would allow to accomplish the task by thermophysical modeling, in particular, for the cases of a tumor located within the ciliary body and adjacent choroid [13, 17-19].

The shape of the human eye is nearly spherical, with deviations from sphericity being small enough to be considered negligible in modeling. The internal structure of the eye is symmetrical with respect to the axis passing through the center of the cornea, lens and vitreous [13]. Therefore, it would be appropriate to consider a model for temperature processes in such structures using spherical polar coordinates.

The heat conduction equation in spherical polar coordinates is as follows [20]:

$$\frac{1}{r^2}\cdot\frac{\partial}{\partial r}(\lambda_r\cdot r^2\cdot\frac{\partial T}{\partial r})+\frac{\partial}{\partial l}(\lambda_\varphi\cdot\frac{\partial T}{\partial l})=-q(r,\varphi)+\rho\cdot c\cdot\frac{\partial T}{\partial t}. \quad (1)$$

Mathematical expressions for temperature function *T(r, φ, t)* can be expressed as analytical formulas only in the simplest case, when the function depends on a single variable, radius (r). In this case, the problem to be solved becomes a centrally symmetrical problem [21].

The finite element method [22] was used to solve equation (3), with curvilinear quadrilateral elements in polar coordinates employed in order to simplify algorithms for mesh generation and numbering the nodes of finite-element meshes.

Quadrilateral elements can be approximated with hyperboloidal surfaces, and the temperature function *T(r, z, t)* relevant to each element can be approximated by a quadratic function. A quadrilateral element is described in space by 8 nodes located at the element corners and midsides, and quadratic approximation is performed with quadratic parabolas located at these nodes. Quadratic functions show much similarity with a function of temperature *T(r, φ)* in a physical system with regard to spatial distribution.

The so called coordinate functions in relative coordinates (*ζ, η*) are used for implementation of approximation, and in case of a square expressed coordinates (*ζ, η,* T), these functions are expressed as follows [23]:

for the nodes located at the corner points (i = 1,3,5,7),

$$N_i(\xi,\eta)=0.25\cdot(1+\xi_i\xi)\cdot(1+\eta_i\eta)\cdot(\xi_i\xi+\eta_i\eta-1);$$

for the nodes located at the middle points of the horizontal sides of the square (i = 2,6),

$$N_i(\xi,\eta)=0.5\cdot(1-\xi^2)\cdot(1+\eta_i\eta);$$

and

for the nodes located at the middle points of the vertical sides of the square (i = 4,8),

$$N_i(\xi,\eta)=0.5\cdot(1-\eta^2)\cdot(1+\xi_i\xi).$$

Coordinate functions equal 1 at eigennodes and equal 0 at any other nodes. In addition, an algebraic sum of coordinate functions for all the nodes of a finite element equals 1: $\sum_{i=1}^{8}N_i(\xi,\eta)=1.$

Coordinate functions perform mapping of a square, expressed in relative coordinates (*ζ, η*), onto a curvilinear quadrilateral, expressed in absolute coordinates (r, *φ*). Coordinate transformation is performed as follows:

$$r=\sum_{i=1}^{8}N_i(\xi,\eta)\cdot r_i;\ \varphi=\sum_{i=1}^{8}N_i(\xi,\eta)\cdot\varphi_i, \quad (2)$$

where r_i and φ_i are coordinates of finite element nodes expressed in the (r, φ) system.

One may use coordinate functions in order to transform the heat conduction equation (1) in the unknown function T(r, *φ*) into the system of linear algebraic equations in the unknown values of this function at approximation nodes:

$$[K+H]\cdot[T]=[F]+[C]\cdot\left[\frac{dT}{dt}\right]+[H]\cdot[T_0]. \quad (3) \qquad (3)$$

Components of the matrices of finite-element equation system (3) expressed in spherical polar coordinates are calculated through coordinate functions:

for the coefficient matrix,

$$k_{ij}=\lambda_r\cdot\iint_{\varphi\ r}\frac{dN_i}{dr}\cdot\frac{dN_j}{dr}\cdot r^3\cdot dr\cdot d\varphi+\lambda_\varphi\cdot\iint_{\varphi\ r}\frac{dN_i}{dz}\cdot\frac{dN_j}{dz}\cdot r^3\cdot dr\cdot d\varphi;$$

for the free-term matrix,

$$f_i=-\iint_{\varphi\ r}N_i\cdot q_i(r,\varphi)\cdot r^3\cdot dr\cdot d\varphi;$$

and for the heat capacity matrix,

$$c_{ij}=\rho\cdot c\cdot\iint_{\varphi\ r}N_i\cdot N_j\cdot r^3\cdot dr\cdot d\varphi.$$

The components taking into account convective cooling of the ocular surface are integrated only over the angular coordinate, with the eye-globe radius R being constant. Therefore,

$$h_{ij}=R^3\cdot\int_{\varphi}N_i\cdot N_j\cdot\alpha_r(\varphi)\cdot d\varphi.$$

In addition, matrix equation (3) is written for the condition that the cornea and the exposed scleral surface are in contact with ambient air, the unexposed sclera surface is surrounded by orbital tissues, and these media differ in temperature. In this equation $[T_0]$ is the ambient temperature matrix for the relevant finite-element nodes on the integration surface.

The Crank-Nicolson scheme [23] in a matrix form is used to solve non-stationary problems:

$$\left[\frac{1}{2}\cdot[K+H]+\frac{1}{\Delta t}\cdot[C]\right]\cdot[T_{j+1}]=[F_j]-\left[\frac{1}{2}\cdot[K+H]-\frac{1}{\Delta t}\cdot[C]\right]\cdot[T_j]+[H]\cdot[T_0]. \quad (4)$$

The model was implemented as a BASIC language computer program that provides calculation of thermal conditions in the human eye based on the following input parameters:

tn, baseline temperature in various ocular compartments;

t0, ambient temperature;

dt, integration step for the cryogenic destruction process (1 to 3 seconds);

mL, number of integration steps;

Rg, average eye globe radius based on ultrasound measurements (mm);

dsc, average scleral thickness based on ultrasound measurements (mm);

dblu, average choroidal thickness based on ultrasound measurements (mm);

dse, average retinal thickness based on ultrasound measurements (mm);

f1, distance from the centre of the cornea to the limbus (mm);

f2, distance from the limbus to the (mm);

f3, distance from the tip of the cryoprobe to the conjunctival fornix (mm).

The software will split the domain under investigation into finite elements, and assign thermal physical characteristics to each finite element of the mesh (as per Table 1) automatically. This makes operating the software easy; however, the location of the target tumor and type of the cryogenic unit are limitations of the software. While the software is running, it will display plots for radial isotherms from the probe tip and across the ocular surface. In addition, it will display temperature values at points specified by the user on completion of computations.

Figure 4 shows plots for radial isotherms from the probe tip and across the ocular surface in cryogenic destruction of the conjunctival tumor at second 60 of intensive freezing to illustrate the results of software execution (isotherms are plotted at 8.8 °C intervals).

Discussion

Currently, there are no criteria for dosing the cryogenic exposure in the treatment of epibulbar tumors, which may cause complications in some cases. Peksayar et al [3, 7] have reported that excessive freezing of the tumors located on the corneoscleral limbus and ciliary body resulted in sectorial iris atrophy, ocular hypotony, iritis, and corneal scarring.

Cryotherapy is thought to act by destroying cells initially by its thermal effect and later by obliteration of the microcirculation, resuiting in ischemic infarction of tissues; this is relevant both to superficially located tumors and to deep infiltrating tumors [24].

Currently, a degree of cryogenic exposure for the tumor during cryogenic destruction is determined visually by the surgeon. Peksayar et al [7] have applied cryotherapy on the ocular tissues until the ice ball formed 0.5 to 2 mm around the probe. The intended extension of the ice ball was 2 mm for the conjunctiva, 1 mm for the episcleral tissues and the corneoscleral limbus, and 0.5 mm for the cornea.

In our current study, we used infrared thermography and found that, in cryogenic destruction of epibulbar tumors located in the projection of the ciliary body onto the sclera, initially, the sclera surrounding the centre of freezing gradually cooled down, while the cornea started cooling down rapidly only in 30 to 60 seconds. This phenomenon may indicate (a) the ciliary body in the exposure area is deeply frozen, and (b) the microcirculation is possibly obliterated and stopped functioning as a heat sink, which is consistent with the hypotheses of others [7, 24].

The model (a) was developed while taking into account differences in heat conduction and heat capacity between the sclera, ciliary body and cornea, and (b) also confirmed the above finding. The cornea has no microcirculation of its own, and rapidly loses heat when ciliary body structures undergo deep freezing. However, as expected, corneal regions differed in the rate of cooling down. The corneal site adjacent to the freeze center was the first to begin cooling down, followed by the central cornea.

In addition, our current study demonstrated the potential for real-time imaging and prediction of individual gradual increases in tissue temperature at the freezing centre and in the surrounding tissues. Recording gradual increases in tissue temperature with time at the freezing centre may be useful in cryogenic destruction of large tumors that necessitate a number of sequential freeze-thaw cycles with a control of the time when the ocular temperature returns to baseline.

Conclusion

IRT with FLIR ONE (FLIR® Systems) system allows real-time heat-pattern imaging for the freeze zone during controlled cryogenic destruction of epibulbar tumors located in the projection of the ciliary body onto the sclera. A thermophysical model was developed to determine temperature characteristics of the thermal fields. The developed model allows for the assessment of distribution of temperature gradients in the superficial and underlying tissues in cryogenic destruction of tumors varying in size. We believe that the developed model will allow determining individual cryogenic exposure durations that would prevent excessive freezing of the surrounding structures (in particular, the ciliary body and cornea), thus contributing to reduced post-operative complication rate. In addition, IRT allows for the assessment of gradual post-freezing increases in ocular tissue temperature to the baseline temperature, should a repeat cycle of cryogenic destruction of the tumor be required. Further studies should match individual cryogenic exposure durations computed by the model to the data relating to (a) visual estimates of the freeze zone and (b) clinical outcomes, in order to determine the details of the developed “method for controlled cryogenic destruction of epibulbar tumors” which require correction.

References

1. Divine RD, Anderson RL. Nitrous oxide cryotherapy for intraepithelial epithelioma of the conjunctiva. Arch Ophthalmol. 1983;101(5):782–6.
2. Fraunfelder FT, Wingfield D. Management of intraepithelial conjunctival tumors and squamous cell carcinomas. Am J Ophthalmol. 1983 Mar;95(3):359–63.
3. Peksayar G, Soyturk MK, Demiryont M. Long-term results of cryotherapy on malignant epithelial tumors of the conjunctiva. Am J Ophthalmol. 1989 Apr 15;107(4):337-40.
4. Buiko AS, Safronenkova IA, Elagina VA. [Methodological guidelines for cryogenic and radiocryogenic surgical treatment for malignant epithelial eyelid tumors]. Odessa: Astroprint; 2015. Russian
5. Basti S, Macsai MS. Ocular surface squamous neoplasia: a review. Cornea. 2003;22:687–704.
6. Kenawy N, Lake SL, Coupland SE, et al. Conjunctival melanoma and melanocytic intraepithelial neoplasia. Eye (Lond). 2013;27(2):142–52.
7. Peksayar G, Altan-Yaycioglu R, Onal S. Excision and cryosurgery in the treatment of conjunctival malignant epithelial tumours. Eye (Lond). 2003;17(2): 228–32.
8. Buschmann W. Kryochirurgie von Tumoren in der Augenregion. Stuttgart, New York: Thieme; 1999. pp.56–104.
9. Buĭko AS, Karpovskii EYa, Safronenkova IA et al. [Epithelial tumors of the eyelids: cryosurgery or scalpel?]. Oftalmol Zh. 1991;(6):338–44. Russian
10. Kaczmarek M, Nowakowski A, Suchowirski M, et al. Active dynamic thermography in cardiosurgery. Quant Infr Therm J. 2007;4(1):107–23
11. Kawasaki S, Mizoue S, Yamaguchi M, Shiraishi A, et al. Evaluation of filtering bleb function by thermography. Br J Ophthalmol. 2009 Oct;93(10):1331-6.
12. Tan JH, Ng EYK, Rajendra Acharya U. Infrared thermography on ocular surface temperature: a review. Infrared Phys Technol. 2009;52:97–108.
13. Anatychuk LI, Pasechnikova NV, Kobylianskyi RR, et al. Computer simulation of thermal processes in human eye. Journal of Thermoelectricity. 2017;(5):41–58. Russian
14. Ooi EH, Ng EYK. Ocular temperature distribution: a mathematical perspective. J Mech Med Biol. 2009;9(2):199–227.
15. Buĭko AS, Elagina VA, Landa Iu. [Potentials for increasing the effectiveness of cryogenic treatment of eyelid tumors using a device based on an adjustable balloon throttle microcryogenic system]. Oftalmol Zh. 1987;(5):272–6. Russian
16. Zadorozhnyy OS, Guzun OV, Brarishko AIu, et al. Infrared thermography of external ocular surface in patients with absolute glaucoma in transscleral cyclophotocoagulation: a pilot study. J Ophthalmol (Ukraine). 2018; (2):23–8.
17. Mapstone R. Determinants of ocular temperature. Br J Ophthalmol. 1968;52:729–41.
18. Vit VV. [The structure of the human visual system]. Odessa: Astroprint; 2003. Russian
19. Scott JA. A finite element model of heat transport in the human eye. Phys Med Biol. 1988; 33: 227–41.
20. Karlslow HS, Jaeger JC. [Conduction of Heat in Solids]. Moscow: Nauka; 1964. Russian
21. Savin SN. [Modeling the epoxy cure processes in spherical layers]. Visnyk ONU. Khimiia. 2013;18(4):38–45. Russian
22. Segerlind LJ. [Applied Finite Element Analysis]. Moscow: Mir; 1979. Russian
23. Altoiz BA, Savin NV, Shatagina EA. [Effect of heat release in a microinterlayer of a liquid on the measurement of its viscosity]. Zhurnal Tekhnicheskoi Fiziki. 2014; 59 (5):21–7. Russian
24. Lee GA, Hirst LW. Ocular surface squamous neoplasia. Surv Ophthalmol. 1995 May-Jun;39(6):429–50.

Table 1. Thermal physical characteristics of ocular structures

Ocular structures	Heat conduction W/(m•K)	Density kg/m^3	Heat capacity J/(kg•K)
Cornea	0.580	1050	4178
Aqueous humor of the anterior chamber	0.580	1000	3997
Lens	0.400	1050	3000
Vitreous body	0.603	1000	4178
Retina	0.628	1000	4190
Blood	0.53-0.55	1050	4050

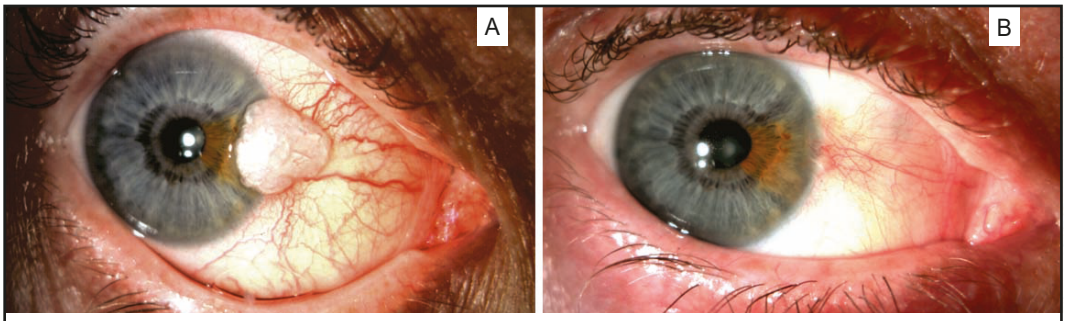

Fig. 1. A: Carcinoma in situ of the scleral, limbal conjunctiva and cornea in the right eye. B: The same eye 3 months after cryogenic destruction of the tumor. No deformation of the pupil is observed.

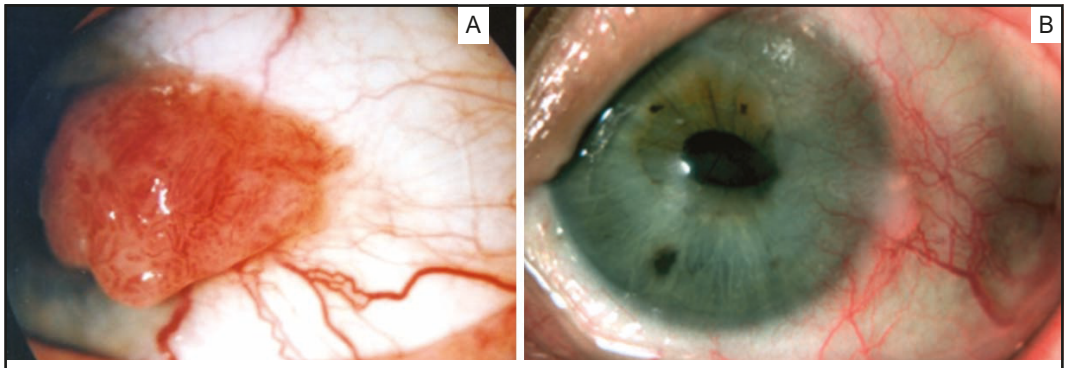

Fig. 2. A: Conjunctival melanoma located in the projection of the ciliary body. B: The same eye 3 months after cryogenic destruction of the tumor. Deformation of the pupil and focal opacity in the corneal periphery are observed.

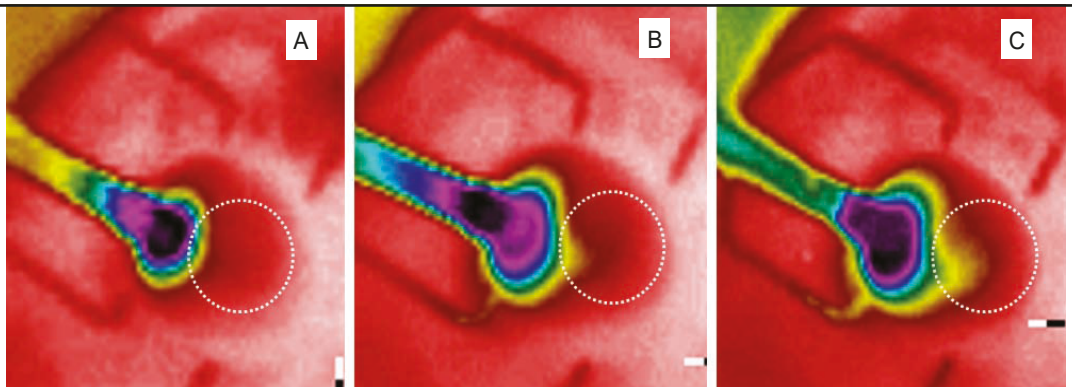

Fig. 3. A: Thermal pattern of the eye with epibulbar tumor located in the projection of the ciliary body 30 seconds after initiation of the procedure. The tissue surrounding the centre of exposure is seen to uniformly cool down. The cornea is highlighted with dashed line. B: Thermal pattern 60 seconds after initiation of the procedure. An insubstantial local reduction in corneal temperature is observed. C: Thermal pattern 75 seconds after initiation of the procedure. A progressive reduction in corneal temperature is observed.

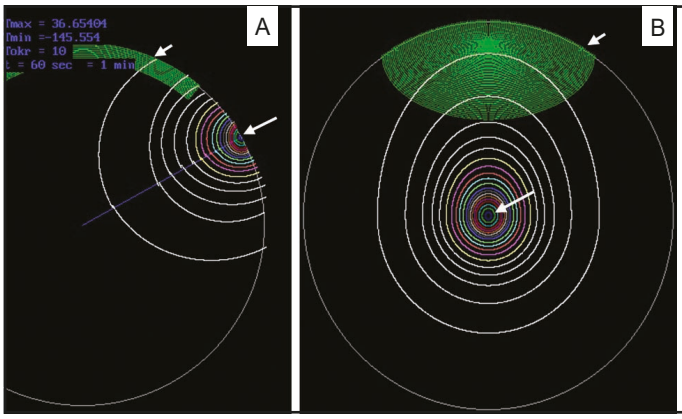

Fig. 4. Depth distribution of isotherms (A) and ocular surface distribution of isotherms (B) in cryogenic destruction of the conjunctival tumor (short arrow points to the cornea and long arrow points to the freeze center).